
Accelerating Diffusion Models via Early Stop of the Diffusion Process

Zhaoyang Lyu^{1,2} Xudong Xu^{1,2} Ceyuan Yang^{1,2} Dahua Lin^{1,2} Bo Dai²

¹The Chinese University of Hong Kong

²Shanghai AI Laboratory

lyuzhaoyang@link.cuhk.edu.hk, xx018@ie.cuhk.edu.hk
 yc019@ie.cuhk.edu.hk, dhlin@ie.cuhk.edu.hk, daibo@pjlab.org.cn

Abstract

Denoising Diffusion Probabilistic Models (DDPMs) have achieved impressive performance on various generation tasks. By modeling the reverse process of gradually diffusing the data distribution into a Gaussian distribution, generating a sample in DDPMs can be regarded as iteratively denoising a randomly sampled Gaussian noise. However, in practice DDPMs often need hundreds or even thousands of denoising steps to obtain a high-quality sample from the Gaussian noise, leading to extremely low inference efficiency. In this work, we propose a principled acceleration strategy, referred to as Early-Stopped DDPM (ES-DDPM), for DDPMs. The key idea is to stop the diffusion process early where only the few initial diffusing steps are considered and the reverse denoising process starts from a non-Gaussian distribution. By further adopting a powerful pre-trained generative model, such as GAN and VAE, in ES-DDPM, sampling from the target non-Gaussian distribution can be efficiently achieved by diffusing samples obtained from the pre-trained generative model. In this way, the number of required denoising steps is significantly reduced. In the meantime, the sample quality of ES-DDPM also improves substantially, outperforming both the vanilla DDPM and the adopted pre-trained generative model. On extensive experiments across CIFAR-10, CelebA, ImageNet, LSUN-Bedroom and LSUN-Cat, ES-DDPM obtains promising acceleration effect and performance improvement over representative baseline methods. Moreover, ES-DDPM also demonstrates several attractive properties, including being orthogonal to existing acceleration methods, as well as simultaneously enabling both global semantic and local pixel-level control in image generation.

1 Introduction

Denoising Diffusion Probabilistic Models (DDPMs) Sohl-Dickstein et al. (2015) are a class of generative models that have received growing attention in recent years, due to their promising results in both unconditional and conditional generation tasks, such as image generation (Ho et al., 2020; Dhariwal & Nichol, 2021; Nichol et al., 2021), image manipulation and restoration (Nichol et al., 2021; Meng et al., 2021; Saharia et al., 2021b,a), audio generation (Chen et al., 2020; Kong et al., 2020), as well as 3D shape generation and completion (Luo & Hu, 2021; Zhou et al., 2021; Lyu et al., 2022; Zhou et al., 2021). DDPMs regard the generation procedure as the reverse of a diffusion process, which gradually adds noises to data samples and transforms the data distribution into a Gaussian distribution. Therefore, synthesizing a sample from DDPMs is achieved by denoising a randomly sampled Gaussian noise iteratively.

While DDPMs show great potential in various generation tasks, one major issue of them is their intrinsic low inference efficiency, as obtaining a high quality sample from the vanilla DDPM usually requires thousands of iterative denoising steps, each of which involves a forward evaluation of the

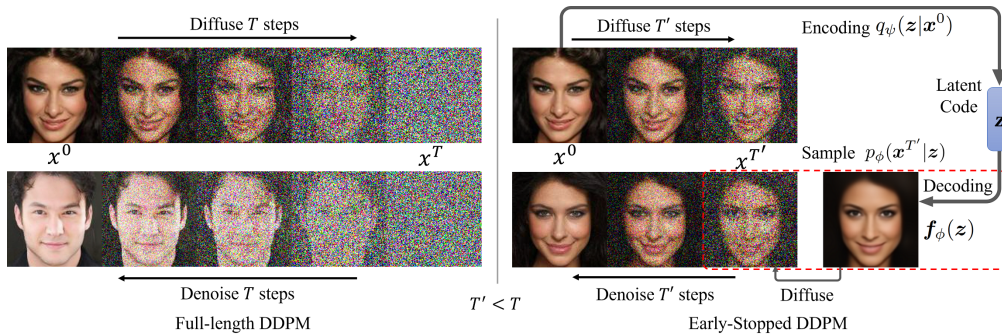


Figure 1: Compare Early-Stopped DDPM (ES-DDPM) with the full-length DDPM.

underlying neural network. To accelerate DDPMs, previous attempts (Ho et al., 2020; Kong & Ping, 2021; Nichol & Dhariwal, 2021) propose to integrate multiple standard denoising steps into a single jumping denoising step. Although the number of denoising steps is reduced, such integrated denoising steps break the Gaussian assumption of DDPMs’ denoising process (Xiao et al., 2021; Sohl-Dickstein et al., 2015), resulting in dropped sample quality. On the other hand, acceleration of DDPMs is also indirectly achieved by (Preechakul et al., 2021; Pandey et al., 2022), which inject image features or VAE-generated images into the denoising process as additional conditions. Such conditioned denoising processes are more effective than the original one, requiring fewer denoising steps to obtain a high-quality sample. However, their acceleration effect is often limited in practice since there are no modifications to the vanilla conditional DDPM generation framework in these approaches. It thus remains a challenging task to accelerate DDPMs in a principled way without compromising the quality of synthesized samples, especially for unconditional generation or class-conditioned generation, where no strong conditioning signal is available.

In this work, we propose a novel acceleration strategy for DDPMs that not only boosts the efficiency of DDPMs without breaking any of the assumptions, but also, as an additional benefit, improves the generation quality of DDPMs. The core idea of our strategy, dubbed as **Early-Stopped DDPM (ES-DDPM)**, is stopping the diffusion process early as shown in Figure 1. Instead of diffusing the data distribution into a Gaussian distribution via hundreds to thousands of iterative steps, ES-DDPM considers only the initial few diffusion steps, so that the reverse denoising process starts from a non-Gaussian distribution q , leading to a significantly reduced number of denoising steps. One remaining issue is ES-DDPM requires sampling from the non-Gaussian distribution q to generate data samples, yet q has no closed form formulations. To overcome this issue, we observe that q is diffused from the real data distribution, in the meantime many of existing generative models provide a good approximation of the real data distribution. Consequently, we further equip ES-DDPM with a pre-trained generative model (e.g. GAN (Karras et al., 2019) and VAE (Kingma & Welling, 2013)) so that sampling from q becomes diffusing samples obtained from the pre-trained generative model. Since both the sampling and the diffusion operation can be easily achieved in a single step, the pre-trained generative model brings only minor computational overhead to ES-DDPM.

The proposed ES-DDPM bears several important advantages. **1)** The number of denoising steps in ES-DDPM is significantly reduced (from 1000 steps to 100 steps in the best case of our experiments). Moreover, such acceleration effect is achieved without sacrificing the quality of generated samples. In fact, by combining a pre-trained generative model, ES-DDPM outperforms both the vanilla DDPM as well as the pre-trained generative model in terms of sample quality. **2)** Unlike the acceleration strategies based on jumping denoising steps that only accelerates the generation process during inference, ES-DDPM provides a principled way to accelerate DDPMs in both training and inference. **3)** While major properties of the vanilla DDPM is preserved in ES-DDPM, it is orthogonal to most existing acceleration strategies of DDPMs. As shown in our experiments, ES-DDPM coupled with other acceleration strategies results in further improved acceleration effect. **4)** ES-DDPM not only maintains the properties of the vanilla DDPM, it also enjoys the properties of the involved pre-trained generative model. For instance, when combined with a StyleGAN2 for unconditional image generation, ES-DDPM enables both global semantic control and local pixel-level control over generated images, as shown in our experiments.

2 Background on DDPMs

In Denoising Diffusion Probabilistic Models (DDPMs), the diffusion process is defined as

$$q(\mathbf{x}^{1:T}|\mathbf{x}^0) = \prod_{t=1}^T q(\mathbf{x}^t|\mathbf{x}^{t-1}), \text{ where } q(\mathbf{x}^t|\mathbf{x}^{t-1}) = \mathcal{N}(\mathbf{x}^t; \sqrt{1 - \beta_t}\mathbf{x}^{t-1}, \beta_t\mathbf{I}), \quad (1)$$

where β_t 's are some predefined small constants, and $\mathbf{x}^{1:T}$ denotes the set of variables $\{\mathbf{x}^1, \mathbf{x}^2, \dots, \mathbf{x}^T\}$. Similar notations are used to denote a set of variables in rest part of the paper. In the diffusion process, we gradually add noise to the clean image \mathbf{x}^0 . T is set to be a sufficiently large number so that \mathbf{x}^T is close to a Gaussian noise. $T = 1000 \sim 4000$ is a typical choice for most works. The reverse process is defined as

$$p_\theta(\mathbf{x}^{0:(T-1)}|\mathbf{x}^T) = \prod_{t=1}^T p_\theta(\mathbf{x}^{t-1}|\mathbf{x}^t), \text{ where } p_\theta(\mathbf{x}^{t-1}|\mathbf{x}^t) = \mathcal{N}(\mathbf{x}^{t-1}; \boldsymbol{\mu}_\theta(\mathbf{x}^t, t), \sigma_t^2 \mathbf{I}). \quad (2)$$

The variance σ_t^2 's can be set as time-step dependent constants or learned by a neural network. The mean is parameterized by a neural network $\boldsymbol{\mu}_\theta(\mathbf{x}^t, t)$. The neural network is trained to simulate the reverse process of the diffusion process defined in Equation 1. To generate an image from the reverse process, we first sample \mathbf{x}^T from the Gaussian distribution, and then sample \mathbf{x}^{t-1} from $p_\theta(\mathbf{x}^{t-1}|\mathbf{x}^t)$ for $t = T, T-1, \dots, 1$. \mathbf{x}^0 is the image that the DDPM generates.

The generation process of a DDPM is extremely slow as it need to sample from the transition distribution $p_\theta(\mathbf{x}^{t-1}|\mathbf{x}^t)$ iteratively, which involves hundreds or even thousands of evaluations of the output of the neural network $\boldsymbol{\mu}_\theta(\mathbf{x}^t, t)$.

3 Methodology

It is necessary to accelerate the sampling process of the DDPM for any practical usage. Our key insight is that we do not need to diffuse a clean image thousands of steps to turn it into a Gaussian noise as shown in Equation 1. We can adopt early stop in the diffusion process as shown in Figure 1. We cut the diffusion process in the middle at $t = T' < T$, and use an encoder to encode the noisy image $\mathbf{x}^{T'}$ into a low dimension vector \mathbf{z} in one step. Correspondingly, in the sampling process, we first sample a latent code \mathbf{z} from the Gaussian distribution, then use a decoder to sample $\mathbf{x}^{T'}$ from \mathbf{z} . Finally, we use the DDPM to denoise $\mathbf{x}^{T'}$ to a clean image \mathbf{x}^0 in fewer steps than the original sampling process. We name the cut DDPM **early-stopped DDPM (ES-DDPM)**.

Our encoding process, which encodes the clean image \mathbf{x}^0 to a low dimension latent code \mathbf{z} , is defined as

$$q(\mathbf{x}^{1:T'}, \mathbf{z}|\mathbf{x}^0) = q(\mathbf{x}^{1:T'}|\mathbf{x}^0)q_\psi(\mathbf{z}|\mathbf{x}^{1:T'}, \mathbf{x}^0) = q(\mathbf{x}^{1:T'}|\mathbf{x}^0)q_\psi(\mathbf{z}|\mathbf{x}^0), \quad (3)$$

where $q_\psi(\mathbf{z}|\mathbf{x}^0)$ is the encoder. We set it to a Gaussian distribution whose mean and standard deviation are parameterized by a neural network. $q(\mathbf{x}^{1:T'}|\mathbf{x}^0)$ is a partial diffusion process of Equation 1, and it is defined as

$$q(\mathbf{x}^{1:T'}|\mathbf{x}^0) = \prod_{t=1}^{T'} q(\mathbf{x}^t|\mathbf{x}^{t-1}), \text{ where } q(\mathbf{x}^t|\mathbf{x}^{t-1}) = \mathcal{N}(\mathbf{x}^t; \sqrt{1 - \beta_t} \mathbf{x}^{t-1}, \beta_t \mathbf{I}). \quad (4)$$

In this partial diffusion process, we do not need T' to be large enough to guarantee that $\mathbf{x}^{T'}$ is close to a Gaussian noise.

We define the sampling process as

$$p(\mathbf{x}^{0:T'}, \mathbf{z}) = p(\mathbf{z})p_\phi(\mathbf{x}^{T'}|\mathbf{z})p_\theta(\mathbf{x}^{0:(T'-1)}|\mathbf{x}^{T'}), \quad (5)$$

where $p(\mathbf{z})$ is assumed to follow standard Gaussian distribution, $p_\phi(\mathbf{x}^{T'}|\mathbf{z})$ is the decoder parameterized by a neural network, and $p_\theta(\mathbf{x}^{0:(T'-1)}|\mathbf{x}^{T'})$ is the reverse process of the partial diffusion process in Equation 4. It is defined as

$$p_\theta(\mathbf{x}^{0:(T'-1)}|\mathbf{x}^{T'}) = \prod_{t=1}^{T'} p_\theta(\mathbf{x}^{t-1}|\mathbf{x}^t), \text{ where } p_\theta(\mathbf{x}^{t-1}|\mathbf{x}^t) = \mathcal{N}(\mathbf{x}^{t-1}; \boldsymbol{\mu}_\theta(\mathbf{x}^t, t), \sigma_t^2 \mathbf{I}). \quad (6)$$

Through variational inference, we can prove that

$$\log p(\mathbf{x}^0) \geq -(L_{\text{VAE}} + L_{\text{DDPM}}), \quad (7)$$

where $L_{\text{VAE}} = D_{\text{KL}}(q_\psi(z|\mathbf{x}^0)||p(z)) + \mathbb{E}_{q_\psi(z|\mathbf{x}^0)} D_{\text{KL}}(q(\mathbf{x}^{T'}|\mathbf{x}^0)||p_\phi(\mathbf{x}^{T'}|z)),$ (8)

$$L_{\text{DDPM}} = \sum_{t=2}^{T'} \mathbb{E}_{q(\mathbf{x}^t|\mathbf{x}^0)} D_{\text{KL}}(q(\mathbf{x}^{t-1}|\mathbf{x}^t, \mathbf{x}^0)||p_\theta(\mathbf{x}^{t-1}|\mathbf{x}^t)) - \mathbb{E}_{q(\mathbf{x}^1|\mathbf{x}^0)} \log p_\theta(\mathbf{x}^0|\mathbf{x}^1). \quad (9)$$

D_{KL} denotes Kullback–Leibler divergence. See complete proof in Appendix Section A.1. To maximize the data log-likelihood $\log p(\mathbf{x}^0)$, we need to minimize the two loss terms: L_{DDPM} and L_{VAE} . We will demonstrate that this means we can train an ES-DDPM and a variational autoencoder (VAE) separately, and then combine them together to obtain a new generative model. First, The loss term L_{DDPM} is the same of a normal DDPM, except that we do not need to train the full Markov chain range from 1 to T . Instead, we only need to train the first several steps range from 1 to T' . A normal DDPM trained on the loss of full T terms would also fulfil the requirements here, but as we will show in later experiments, the training process of an ES-DDPM is faster than a normal full-length DDPM.

Next, we show that the loss term L_{VAE} amounts to train a VAE on the clean images \mathbf{x}^0 in the dataset. The first term in L_{VAE} is the same as in a standard VAE, which requires the encoder to encode clean images to a latent space that follows the Gaussian distribution. The second term in L_{VAE} means that we want $p_\phi(\mathbf{x}^{T'}|z)$ to match $q(\mathbf{x}^{T'}|\mathbf{x}^0)$ as close as possible. It is proven by previous works (Sohl-Dickstein et al., 2015; Ho et al., 2020) that

$$q(\mathbf{x}^{T'}|\mathbf{x}^0) \sim N(\mathbf{x}^{T'}; \sqrt{\bar{\alpha}_t}\mathbf{x}^0, (1 - \bar{\alpha}_t)\mathbf{I}), \text{ where } \alpha_t = 1 - \beta_t, \bar{\alpha}_t = \prod_{i=1}^t \alpha_i. \quad (10)$$

Correspondingly, we choose to set $p_\phi(\mathbf{x}^{T'}|z)$ to

$$p_\phi(\mathbf{x}^{T'}|z) \sim N(\mathbf{x}^{T'}; \sqrt{\bar{\alpha}_t}\mathbf{f}_\phi(z), (1 - \bar{\alpha}_t)\mathbf{I}). \quad (11)$$

Then

$$D_{\text{KL}}(q(\mathbf{x}^{T'}|\mathbf{x}^0)||p_\phi(\mathbf{x}^{T'}|z)) = C_1\|\mathbf{x}^0 - \mathbf{f}_\phi(z)\|^2 + C_2, \quad (12)$$

where C_1, C_2 are some scalar constants. Now the second term in L_{VAE} means that the decoder $\mathbf{f}_\phi(z)$ need to reconstruct the original clean image \mathbf{x}^0 , based on the latent code z sampled from the encoder $q_\psi(z|\mathbf{x}^0)$. This is exactly the same procedure as training a VAE on clean images \mathbf{x}^0 in the dataset.

Sampling Procedure. After training the ES-DDPM and the VAE separately, we can combine them to form a new generative model. We follow Equation 5 to generate samples and it is illustrated in Figure 1: First sample z from the standard Gaussian distribution, then use the decoder of the VAE to generate an image $\mathbf{f}_\phi(z)$. Next, sample $\mathbf{x}^{T'}$ from the distribution described in Equation 11. Finally, use the ES-DDPM to sample \mathbf{x}^{t-1} from $p_\theta(\mathbf{x}^{t-1}|\mathbf{x}^t)$ for $t = T', T' - 1, \dots, 1$, and output the generated image \mathbf{x}^0 .

Note that in the above sampling process, we only need to use the decoder $\mathbf{f}_\phi(z)$, while the encoder $q_\psi(z|\mathbf{x}^0)$ is not used. This means that we can not only combine the ES-DDPM with a VAE, but also with any generative model that can map the latent code z to a clean image, such as a GAN. Since after a GAN is trained, its generator is pretty much like the decoder of a VAE, except that the generator’s encoder is not known, but we simply do not need the encoder to generate samples from the combined model. Therefore, we can also think of $\mathbf{f}_\phi(z)$ as the generator of a trained GAN. In fact, we will demonstrate that combining an ES-DDPM with a GAN is more effective than combining it with a VAE in later experiments. For conditional generation tasks, we can also combine a conditional ES-DDPM with a conditional VAE or GAN to achieve acceleration. See details in Appendix A.2.

4 Related Works

Several works (Ho et al., 2020; Kong & Ping, 2021; Nichol & Dhariwal, 2021) propose to accelerate the sampling procedure of DDPMs by making jumping steps in the reverse steps. Watson et al. (2021) propose a dynamic programming algorithm that finds the optimal denoising time-step schedule for DDPMs. Watson et al. (2021) optimize DDPM fast samplers by differentiating through sample quality scores. Salimans & Ho (2022) propose to progressively distill a trained DDPM for fast sampling. Xiao et al. (2021) propose denoising diffusion GANs that can balance sample quality, mode coverage,

and fast sampling. We think our method is orthogonal to these acceleration methods. In principle, these methods can be coupled with our method to accelerate the T' denoising steps in our ES-DDPM.

Some works find that combining DDPMs with VAEs can help accelerate the sampling process of DDPMs. Preechakul et al. (2021) condition the reverse process of the DDPM on an encoded vector of an image. Pandey et al. (2022) condition the reverse process of the DDPM on a reconstructed image by a VAE. Kingma et al. (2021) design variational diffusion models that can generate images in fewer steps than a DDPM. However, all of them still need a complete diffusion process to destroy the input image, and in their sampling process, they still need to run the full denoising process that starts with a Gaussian noise or a very noisy image. In comparison, we adopt early stop in the diffusion process, and we start from a partially diffused image generated by a VAE or GAN in our denoising process. Another major difference is that these methods need to alter the training process and train a DDPM that is specific to the VAE model they want to combine with, while our method can combine a pre-trained DDPM with any other generative models.

We find that a concurrent work (Zheng et al., 2022) adopts a similar acceleration method to our ES-DDPM, where ES-DDPM represents the non-Gaussian distribution of $x^{T'}$ by diffusing clean samples obtained from a pre-trained generative model, while the concurrent work proposes to directly learn the distribution of $x^{T'}$ with a GAN or a conditional transport. Consequently, ES-DDPM bears the following advantages: First, by diffusing the real data distribution approximated by a pre-trained generative model, ES-DDPM avoids learning the distribution of $x^{T'}$ directly, which brings extra computational complexity, and learning the distribution of noisy images $x^{T'}$ may be harder than learning the real data distribution. Second, ES-DDPM can use the same pre-trained generative model for any value of T' , while the concurrent work requires to learn a new model for each possible value of T' . Third, without re-training, ES-DDPM can easily utilize the widely-available pre-trained generative models in the community, and seamlessly integrate advances in the related fields. In this way, attractive properties, such as controllable generation, possessed by existing generative models can be effectively introduced to DDPMs.

5 Experiments

5.1 Image Generation

In this section, we evaluate the image generation performance of our ES-DDPM and compare it with other generative models.

Datasets. We conduct experiments on CIFAR-10 (Krizhevsky et al., 2009), CelebA (Liu et al., 2015), ImageNet (Russakovsky et al., 2015), LSUN-Bedroom and LSUN-Cat (Yu et al., 2015). For the CelebA dataset, we conduct experiments at two resolutions: 64×64 and 128×128 . For the ImageNet dataset, we use a resolution of 64×64 , and we use 256×256 for the LSUN datasets.

Evaluation Metrics. We use the commonly used Fréchet inception distance (Heusel et al., 2017) (FID) and Inception Score (Salimans et al., 2016) (IS) to evaluate the quality of generated images. We also use Improved Precision and Recall metrics (Kynkäänniemi et al., 2019) to explicitly measure sample fidelity and diversity. sFID (Nash et al., 2021) is also used.

CIFAR-10 Experiment. We combine ES-DDPM with other generative models, *i.e.*, vanilla VAE (Kingma & Welling, 2013), DCGAN (Radford et al., 2015), StyleGAN2 (Karras et al., 2020), and test their performance in terms of unconditional image generation on CIFAR-10 (Krizhevsky et al., 2009) dataset. We use the pre-trained 1000-step DDPM on CIFAR-10 from the work (Ho et al., 2020). We insert the images generated by the other generative model (VAE or GAN) to different steps in the reverse process of the DDPM, namely, use different T' in Equation 5. We report FID of the combined generative models in Table 1.

We can see that DDPM can improve the quality of images generated by the other generative models. And roughly speaking, the larger the number of denoising steps T' is, the better the quality is. This is because $p_\phi(x^{T'}|z)$ in Equation 11 gradually approaches to a standard Gaussian noise as T' increases, and hence the combined model gradually matches the original DDPM as T' increases. Another observation is that we need to combine ES-DDPM with a strong generative model like StyleGAN2 if we want to obtain high quality images in few denoising steps. One rather surprising observation is

Table 1: Unconditional image generation performance on CIFAR-10. We report FID between randomly generated 50000 images by the combined generative model and the training set. $T' = 0$ refers to the original VAE or GAN model. $T' = 1000$ is the original 1000-step DDPM.

Denoising Steps T'	0	100	200	300	400	500	600	700	800	900	1000
VAE+ES-DDPM	158.61	49.62	20.88	11.03	5.96	3.69	3.17	3.15	3.12	3.18	
DCGAN+ES-DDPM	33.31	15.54	9.97	7.21	5.49	3.98	3.37	3.13	3.14	3.24	3.20
StyleGAN2+ES-DDPM	7.18	5.52	5.02	4.60	4.03	3.51	3.26	3.11	3.16	3.17	

Table 2: Performance comparison of CelebA unconditional image generation. “*” means the model is trained by ourselves. For our method and self trained models, we report FID between randomly generated 50000 images and the whole dataset.

CelebA-64	Method	FID
Hybrid Models	StyleGAN2+100-step ES-DDPM (Ours)	3.01
	StyleGAN2+200-step ES-DDPM (Ours)	2.55
	1000-step DiffuseVAE (Pandey et al., 2022)	4.76
Score-based Methods	1000-step DDPM* (Ho et al., 2020)	3.26
	250-step PNDM (Liu et al., 2022)	2.71
	NCSN (Song & Ermon, 2019)	25.30
	NCSNv2 (Song & Ermon, 2020)	10.23
GAN-based Methods	COCO-GAN (Lin et al., 2019)	4.00
	StyleGAN2* (Karras et al., 2020)	4.55
	QA-GAN (Parimala & Channappayya, 2019)	6.42
VAE-based Methods	NCP-VAE (Aneja et al., 2020)	5.25
CelebA-128	Method	FID
Hybrid Models	StyleGAN2+100-step ES-DDPM (Ours)	1.76
	StyleGAN2+200-step ES-DDPM (Ours)	1.79
Score-based Methods	1000-step DDPM* (Ho et al., 2020)	5.65
GAN-based Methods	COCO-GAN (Lin et al., 2019)	5.74
	StyleGAN2* (Karras et al., 2020)	2.13
	PresGAN (Dieng et al., 2019)	29.12

that the combined model can even outperform the original DDPM. In other words, we can combine a DDPM with a less powerful generative model, and with less denoising steps, to obtain a even better combined model, which means we can accelerate the DDPM for free! As we will show in later experiments, the same results can be achieved on other datasets as well.

CelebA Experiment. We combine ES-DDPM with StyleGAN2 and test its performance on the CelebA (Liu et al., 2015) dataset at two resolutions: CelebA-64 and CelebA-128. At each resolution, we train two DDPMs with $T' = 100$ and $T' = 200$ using the loss function in Equation 9, and combine them with a self-trained StyleGAN2, respectively. We compare our combined models with self-trained 1000-step DDPMs and other generative models in Table 2. The DDPMs are trained with a linear β schedule following the same procedures in the works (Ho et al., 2020; Song et al., 2020). We can see that when combined with StyleGAN2, our ES-DDPM can achieve lower FIDs than the original DDPM and other score-based methods in even less denoising steps.

Compared with CIFAR-10 experiment results in Table 1, we find that ES-DDPM combined with StyleGAN2 can outperform the full-length DDPM in much less denoising steps on the CelebA dataset. In Table 2, $T' = 100$ or $T' = 200$ can already outperform the 1000-step DDPM, while in Table 1, we need 700 to 800 denoising steps to achieve a lower FID than the full-length DDPM. We think it is because CIFAR-10 is a multi-category dataset while CelebA is a single-category dataset. In other words, CIFAR-10 has more data diversity than CelebA. GANs are known to be able to generate high quality samples, but have poor mode coverage (Zhao et al., 2018; Xiao et al., 2021). On the other hand, DDPMs demonstrate both high sample quality and good mode coverage (Dhariwal & Nichol, 2021). Therefore, for an ES-DDPM to improve the generation diversity of a GAN on a dataset of complex distribution, we need large T' s in Equation 6. Because for small T' s, the ES-DDPM generated image x^0 will be very similar to the GAN generated image $f_\phi(z)$, as there is little diversity and stochasticity in Equation 6 for small T' s. On the other hand, for large T' s, the generated image x^0 can be vastly different from $f_\phi(z)$, because $x^{T'}$ contains very little information of $f_\phi(z)$, and thus the GAN’s generation diversity can be improved. We will explicitly verify this point of view using the Precision and Recall metrics in the following ImageNet and LSUN Experiments.

Table 3: ImageNet-64 class-conditional image generation performance of ES-DDPM+BigGAN-deep. For the DDPM and ES-DDPM experiments, we follow the work (Dhariwal & Nichol, 2021) to use Timestep-Respacing with jumping interval 4. The actual denoising steps is $T'/4$. We do not use classifier guidance.

ES-DDPM Length T'	0(BigGAN-deep)	100	200	300	400	500	600	700	800	900	1000(DDPM)
FID	4.06	3.75	3.47	3.30	3.16	2.92	2.71	2.50	2.31	2.07	2.13
sFID	3.96	3.91	3.96	3.93	3.90	3.83	3.84	3.84	3.84	3.90	4.28
IS	45.00	48.63	50.17	51.45	52.32	53.85	54.41	55.11	55.42	55.29	52.52
Precision	0.795	0.798	0.800	0.794	0.792	0.787	0.784	0.778	0.771	0.756	0.739
Recall	0.483	0.504	0.514	0.529	0.533	0.547	0.565	0.577	0.593	0.608	0.631

Table 4: ES-DDPM+StyleGAN on LSUN-Bedroom.

Denoising Steps T'	0 (StyleGAN)	100	200	300	1000 (DDPM)
FID	2.35	1.85	1.70	1.68	1.86
sFID	6.61	5.93	5.70	5.64	5.75
IS	2.55	2.53	2.54	2.54	2.39
Precision	0.590	0.636	0.642	0.643	0.653
Recall	0.483	0.464	0.472	0.495	0.500

Table 5: ES-DDPM+StyleGAN2 on LSUN-Cat.

Denoising Steps T'	0 (StyleGAN2)	100	200	300	1000 (DDPM)
FID	7.26	5.47	5.15	4.89	5.68
sFID	6.33	6.47	6.57	6.70	6.72
IS	4.84	5.12	5.23	5.33	5.23
Precision	0.576	0.626	0.633	0.631	0.628
Recall	0.432	0.463	0.475	0.489	0.520

ImageNet and LSUN Experiment. For ImageNet-64, we combine ES-DDPM with BigGAN-deep (Brock et al., 2018) and test its class-conditional image generation performance. For LSUN-Bedroom and LSUN-Cat, we combine ES-DDPM with StyleGAN (Karras et al., 2019) and StyleGAN2, respectively. For these experiments, we use pre-trained DDPM models and GAN generated images provided in the work (Dhariwal & Nichol, 2021). The DDPMs are of length 1000 and the variance schedule is learned by a neural network. We follow the same evaluation methods in the work (Dhariwal & Nichol, 2021): FIDs are computed between randomly generated 50000 images and the whole training set. IS’s are computed over the randomly generated 50000 images. Precision and Recall are computed between the randomly generated 50000 images and random 10000 images from the training set.

Experiment results are shown in Table 3, Table 4 and Table 5. Same as CIFAR-10 and CelebA, we can see that ES-DDPM can improve the generation quality of GANs, and the combined model can outperform the original DDPM in terms of FID, sFID and IS. We also observe that BigGAN-deep has low Recall on the complex multi-category ImageNet dataset, its Recall is gradually improved as T' increases. Therefore, the combined model need large T' s around 900 to achieve a lower FID than the full-length DDPM. On the other hand, for the single-category datasets, LSUN-Bedroom and LSUN-Cat, StyleGAN and StyleGAN2 already have a not too bad Recall compared with the full-length DDPMs. Therefore, the ES-DDPMs can improve the GANs’ Recall in less denoising steps, and our combined model can outperform the original full-length DDPM in terms of FID in just 100 steps. In conclusion, for multi-category datasets of complex data distribution, our combined models provide a trade-off between sample diversity and denoising steps. For single-category datasets where GANs already have a good Recall, our combined models provide better sample quality than both the GANs and the original full-length DDPMs, with much fewer denoising steps than the original full-length DDPMs.

5.2 Coupled With Other DDPM Acceleration Methods

Our method can be easily coupled with other DDPM acceleration methods to achieve further acceleration. Recall that our method need to use the ES-DDPM to denoise $x^{T'}$ for T' steps as shown in Equation 6. This denoising process is actually the same as the last T' steps of the reverse process in a normal full-length DDPM. Any method that aims at accelerating the full T -step reverse process of a DDPM, can in principle be applied to accelerate the last T' denoising steps. We use DDIM (Song et al., 2020) and Timestep-Respacing (TR) (Nichol & Dhariwal, 2021) as a demonstration in our experiments. Both DDIM and Timestep-Respacing enable one to sampling from a pre-trained DDPM only on a subsequence of the original denoising steps. We choose a uniform subsequence in our T' denoising steps. We conduct experiments on the CelebA, ImageNet, LSUN-bedroom and LSUN-Cat datasets. CelebA and ImageNet results are shown in Table 6, Table 7. LSUN-bedroom and LSUN-Cat results are shown in Table 8 and Table 9 in Appendix A.4. We can see that our combined model can indeed achieve further acceleration when coupled with other acceleration methods. And compared with other acceleration methods, our combined model bears better sample quality when using the same number of denoising steps in most cases.

5.3 Accelerate Training

We have shown that our combined model can accelerate the sampling process of DDPMs in the previous sections. We also expect our method to be able to accelerate the training process of DDPMs,

Table 6: FID comparison of different DDPM acceleration methods on CelebA. For our models, denoising steps less than 100 steps are achieved by accelerating ES-DDPM($T' = 100$) using DDIM.

		Denoising Steps					
		200	100	50	20	10	5
CelebA-64	ES-DDPM+StyleGAN2+DDIM(Ours)	2.55	3.01	3.97	4.90	6.44	9.15
	DDIM (Song et al., 2020)	-	6.53	9.17	13.73	17.33	-
	FastDPM (Kong & Ping, 2021)	-	7.85	8.31	10.69	15.31	-
	PNDM (Liu et al., 2022)	2.71	2.81	3.34	5.51	7.71	11.3
	Diffusion Autoencoder (Preechakul et al., 2021)	-	5.30	7.05	10.18	12.92	-
	TDPM-GAN (Zheng et al., 2022)	-	3.64	3.28	-	-	-
CelebA-128	ES-DDPM+StyleGAN2+DDIM(Ours)	1.79	1.76	1.86	2.27	3.26	6.15

Table 7: FID and IS comparison of different DDPM acceleration methods on the Imagenet-64 dataset. “*” means the images for evaluation are generated by ourselves for this method.

Denoising Steps	FID					IS				
	25	20	15	10	5	25	20	15	10	5
ES-DDPM($T' = 100$)+BigGAN-deep+TR(Ours)	3.75	3.77	3.80	3.93	4.25	48.63	48.92	49.17	48.81	48.04
DDIM* (Song et al., 2020)	5.90	6.68	8.59	13.48	67.70	38.24	36.72	34.85	30.79	13.17
TR* (Nichol & Dhariwal, 2021)	7.99	11.08	16.49	27.74	78.59	49.62	45.83	39.32	29.32	12.65
DDSS (Watson et al., 2021)	18.40	20.69	24.69	37.32	55.14	18.12	17.92	17.23	14.76	12.90

since we only need to train a denoising chain of length T' , which is shorter than the original denoising chain of length T . This is because our DDPM loss in Equation 9 contains only T' terms, compared with T terms in the original full-length DDPM loss. We compare the training process of our combined models with the full-length 1000-step DDPM on the CelebA dataset. We plot FIDs during the training process of our combined model and the original DDPM in Figure 2. Note that we have already taken into account the training time of the StyleGAN2 by converting the training time of the StyleGAN2 to the equivalent training steps of the DDPM, and it is annotated by a red dashed line in Figure 2. For CelebA-64, we can see that our combined model still converges faster than the full-length DDPM even if we take into account the training time of the StyleGAN2. Specifically, it takes the full-length DDPM 9×10^5 iterations, about 80 hours to achieve an FID of 3.26. In comparison, our ES-DDPM($T' = 100$) only uses 4.5×10^4 iterations, about 4 hours to achieve an FID of 3.09. Even if we take into account the training time of StyleGAN2, which is about 25 hours, the total training time of our combined model (29 hours) is still much shorter than the training time of the full-length DDPM (80 hours). As for CelebA-128, we find the full-length DDPM could not achieve an FID comparable to our combined model even we train it for a very long time.

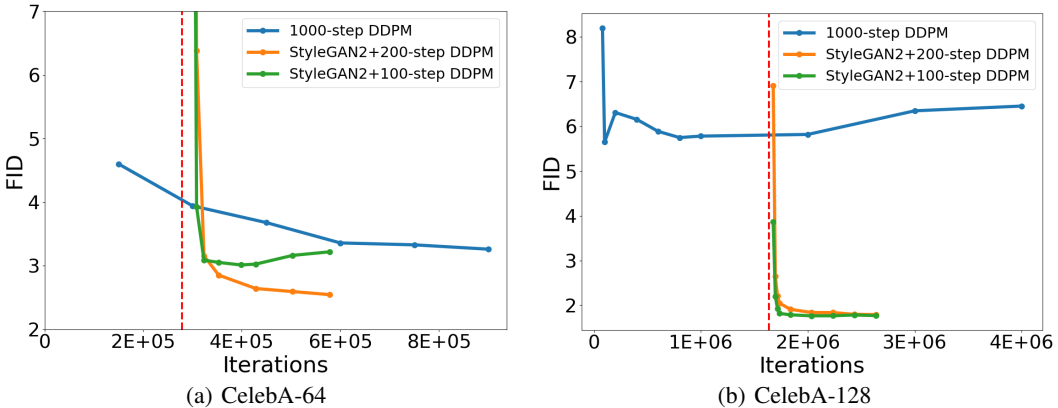


Figure 2: Training time comparison between our combined models and the original full-length DDPMs. DDPMs are trained with batchsize 128 on CelebA-64 and with batchsize 48 on CelebA-128. The red dashed line denotes the training time of StyleGAN2.

5.4 Controllable Image Generation

In previous sections, we have shown that combining GANs and DDPMs can improve their image generation quality, and accelerate the sampling and training process of DDPMs. In this section, we further show that the combined models can benefit from both GANs and DDPMs in terms of controllable generation. DDPMs have achieved impressive results on image local editing (Nichol et al., 2021; Meng et al., 2021). We think this can be largely attributed to DDPMs’ latent space x^t , which has the same dimension as the input image and thus allows us to perform pixel-level manipulation on this latent space. However, this latent space lack semantic meanings to control high-level semantics of the generated image. On the other hand, GANs and VAEs can learn a meaningful

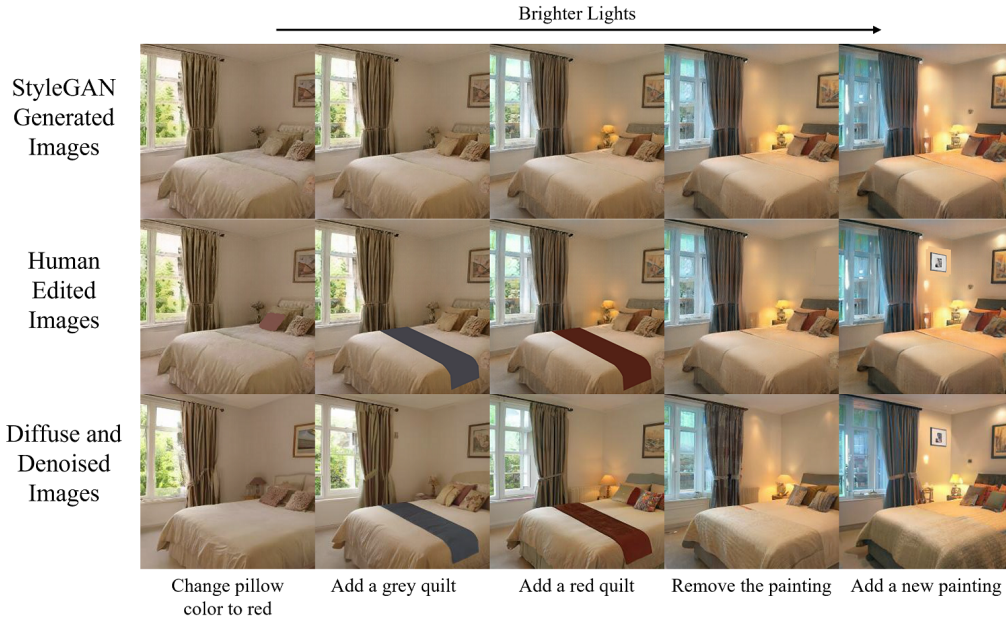


Figure 3: On LSUN-Bedroom-256, we use StyleGAN to control the lighting condition of a bedroom, and then use the ES-DDPM($T' = 200$) to control local details.

representation of an image that can be used to control high-level semantics, but it’s challenging for them to achieve pixel-level control of the generated image. We think that DDPMs and GANs (or VAEs) are complementary to each other in terms of controllable generation. We can achieve both high-level semantic control and pixel-level control of the generated image in our combined models.

It is achieved by following Equation 5 to generate images: First use a GAN or VAE to generate an image $f_\phi(z)$. In this step, the GAN or VAE can control the high-level semantics of the image. Next, we can perform some coarse local editing on the image. Then, sample $x^{T'}$ from the distribution $N(x^{T'}; \sqrt{\alpha_{T'}} f_\phi(z), (1 - \alpha_{T'}) I)$. Finally, use the ES-DDPM to denoise $x^{T'}$ by sampling x^{t-1} from $p_\theta(x^{t-1}|x^t)$ for $t = T', T' - 1, \dots, 1$, and output the generated image x^0 . The denoising process will preserve high-level semantics in $f_\phi(z)$ as long as T' is not too large, and it will refine the local editing we performed and mitigate artifacts in the image.

We conduct experiments to verify the effect of our method on controllable generation. Figure 3 shows that we can use StyleGAN to control the lighting condition of a bedroom, and then perform local editing on the generated images (similar to the stroke-based editing in the work (Meng et al., 2021)). Finally, we use the ES-DDPM to refine the edited images, mitigate artifacts and make the images photo-realistic. In this way, our combined model can control both the high-level lighting condition and local details of the bedroom. Additional examples are provided in Appendix Section A.5.

6 Conclusion

In this work, we propose to adopt early stop in the diffusion process of a DDPM to achieve acceleration. We can combine an early-stopped DDPM with another generative model such as VAE or GAN to obtain a new generative model. The combined model can outperform the original DDPM in terms of sample quality, sampling speed and training speed. We can further accelerate the combined model by coupling it with other DDPM acceleration methods. The combined model also has more control over the generation process. We demonstrate that we can control both high-level semantics and local details of the generated image by combining DDPMs with GANs.

Our method has achieved great acceleration effect and sample quality on single category datasets. However, for multi-category datasets, it still need many denoising steps to outperform the full-length DDPM in terms of sample quality due to the poor mode coverage of GANs. In the future, we could combine ES-DDPM with other generative models that have better mode coverage to achieve high sample quality with less denoising steps on even complex multi-category datasets. In addition, as a generative model, more studies are needed on how to prevent the model from learning biases in the training dataset and from misuse such as deception.

References

- Jyoti Aneja, Alex Schwing, Jan Kautz, and Arash Vahdat. Ncp-vae: Variational autoencoders with noise contrastive priors. 2020.
- Andrew Brock, Jeff Donahue, and Karen Simonyan. Large scale gan training for high fidelity natural image synthesis. *arXiv preprint arXiv:1809.11096*, 2018.
- Nanxin Chen, Yu Zhang, Heiga Zen, Ron J Weiss, Mohammad Norouzi, and William Chan. Wavegrad: Estimating gradients for waveform generation. *arXiv preprint arXiv:2009.00713*, 2020.
- Prafulla Dhariwal and Alexander Nichol. Diffusion models beat gans on image synthesis. *Advances in Neural Information Processing Systems*, 34, 2021.
- Adji B Dieng, Francisco JR Ruiz, David M Blei, and Michalis K Titsias. Prescribed generative adversarial networks. *arXiv preprint arXiv:1910.04302*, 2019.
- Martin Heusel, Hubert Ramsauer, Thomas Unterthiner, Bernhard Nessler, and Sepp Hochreiter. Gans trained by a two time-scale update rule converge to a local nash equilibrium. *Advances in neural information processing systems*, 30, 2017.
- Jonathan Ho, Ajay Jain, and Pieter Abbeel. Denoising diffusion probabilistic models. *Advances in Neural Information Processing Systems*, 33:6840–6851, 2020.
- Tero Karras, Samuli Laine, and Timo Aila. A style-based generator architecture for generative adversarial networks. In *Proceedings of the IEEE/CVF conference on computer vision and pattern recognition*, pp. 4401–4410, 2019.
- Tero Karras, Samuli Laine, Miika Aittala, Janne Hellsten, Jaakko Lehtinen, and Timo Aila. Analyzing and improving the image quality of stylegan. In *Proceedings of the IEEE/CVF conference on computer vision and pattern recognition*, pp. 8110–8119, 2020.
- Diederik P Kingma and Max Welling. Auto-encoding variational bayes. *arXiv preprint arXiv:1312.6114*, 2013.
- Diederik P Kingma, Tim Salimans, Ben Poole, and Jonathan Ho. Variational diffusion models. *arXiv preprint arXiv:2107.00630*, 2021.
- Zhifeng Kong and Wei Ping. On fast sampling of diffusion probabilistic models. *arXiv preprint arXiv:2106.00132*, 2021.
- Zhifeng Kong, Wei Ping, Jiaji Huang, Kexin Zhao, and Bryan Catanzaro. Diffwave: A versatile diffusion model for audio synthesis. *arXiv preprint arXiv:2009.09761*, 2020.
- Alex Krizhevsky, Geoffrey Hinton, et al. Learning multiple layers of features from tiny images. 2009.
- Tuomas Kynkäänniemi, Tero Karras, Samuli Laine, Jaakko Lehtinen, and Timo Aila. Improved precision and recall metric for assessing generative models. *Advances in Neural Information Processing Systems*, 32, 2019.
- Chieh Hubert Lin, Chia-Che Chang, Yu-Sheng Chen, Da-Cheng Juan, Wei Wei, and Hwann-Tzong Chen. Coco-gan: Generation by parts via conditional coordinating. In *Proceedings of the IEEE/CVF international conference on computer vision*, pp. 4512–4521, 2019.
- Luping Liu, Yi Ren, Zhijie Lin, and Zhou Zhao. Pseudo numerical methods for diffusion models on manifolds. In *International Conference on Learning Representations*, 2022. URL <https://openreview.net/forum?id=P1KWVd2yBkY>.
- Ziwei Liu, Ping Luo, Xiaogang Wang, and Xiaoou Tang. Deep learning face attributes in the wild. In *Proceedings of International Conference on Computer Vision (ICCV)*, December 2015.
- Shitong Luo and Wei Hu. Diffusion probabilistic models for 3d point cloud generation. In *Proceedings of the IEEE/CVF Conference on Computer Vision and Pattern Recognition*, pp. 2837–2845, 2021.

- Zhaoyang Lyu, Zhifeng Kong, Xudong XU, Liang Pan, and Dahua Lin. A conditional point diffusion-refinement paradigm for 3d point cloud completion. In *International Conference on Learning Representations*, 2022. URL <https://openreview.net/forum?id=wqD6TfbYkrn>.
- Chenlin Meng, Yutong He, Yang Song, Jiaming Song, Jiajun Wu, Jun-Yan Zhu, and Stefano Ermon. Sdedit: Guided image synthesis and editing with stochastic differential equations. In *International Conference on Learning Representations*, 2021.
- Charlie Nash, Jacob Menick, Sander Dieleman, and Peter W Battaglia. Generating images with sparse representations. *arXiv preprint arXiv:2103.03841*, 2021.
- Alex Nichol, Prafulla Dhariwal, Aditya Ramesh, Pranav Shyam, Pamela Mishkin, Bob McGrew, Ilya Sutskever, and Mark Chen. Glide: Towards photorealistic image generation and editing with text-guided diffusion models. *arXiv preprint arXiv:2112.10741*, 2021.
- Alexander Quinn Nichol and Prafulla Dhariwal. Improved denoising diffusion probabilistic models. In *International Conference on Machine Learning*, pp. 8162–8171. PMLR, 2021.
- Kushagra Pandey, Avideep Mukherjee, Piyush Rai, and Abhishek Kumar. Diffusevae: Efficient, controllable and high-fidelity generation from low-dimensional latents. *arXiv preprint arXiv:2201.00308*, 2022.
- Kancharla Parimala and Sumohana Channappayya. Quality aware generative adversarial networks. *Advances in neural information processing systems*, 32, 2019.
- Konpat Preechakul, Nattanat Chatthee, Suttisak Wizadwongsa, and Supasorn Suwajanakorn. Diffusion autoencoders: Toward a meaningful and decodable representation. *arXiv preprint arXiv:2111.15640*, 2021.
- Alec Radford, Luke Metz, and Soumith Chintala. Unsupervised representation learning with deep convolutional generative adversarial networks. *arXiv preprint arXiv:1511.06434*, 2015.
- Olga Russakovsky, Jia Deng, Hao Su, Jonathan Krause, Sanjeev Satheesh, Sean Ma, Zhiheng Huang, Andrej Karpathy, Aditya Khosla, Michael Bernstein, et al. Imagenet large scale visual recognition challenge. *International journal of computer vision*, 115(3):211–252, 2015.
- Chitwan Saharia, William Chan, Huiwen Chang, Chris A Lee, Jonathan Ho, Tim Salimans, David J Fleet, and Mohammad Norouzi. Palette: Image-to-image diffusion models. *arXiv preprint arXiv:2111.05826*, 2021a.
- Chitwan Saharia, Jonathan Ho, William Chan, Tim Salimans, David J Fleet, and Mohammad Norouzi. Image super-resolution via iterative refinement. *arXiv preprint arXiv:2104.07636*, 2021b.
- Tim Salimans and Jonathan Ho. Progressive distillation for fast sampling of diffusion models. *arXiv preprint arXiv:2202.00512*, 2022.
- Tim Salimans, Ian Goodfellow, Wojciech Zaremba, Vicki Cheung, Alec Radford, and Xi Chen. Improved techniques for training gans. *Advances in neural information processing systems*, 29, 2016.
- Jascha Sohl-Dickstein, Eric Weiss, Niru Maheswaranathan, and Surya Ganguli. Deep unsupervised learning using nonequilibrium thermodynamics. In *International Conference on Machine Learning*, pp. 2256–2265. PMLR, 2015.
- Jiaming Song, Chenlin Meng, and Stefano Ermon. Denoising diffusion implicit models. *arXiv preprint arXiv:2010.02502*, 2020.
- Yang Song and Stefano Ermon. Generative modeling by estimating gradients of the data distribution. *Advances in Neural Information Processing Systems*, 32, 2019.
- Yang Song and Stefano Ermon. Improved techniques for training score-based generative models. *Advances in neural information processing systems*, 33:12438–12448, 2020.

Daniel Watson, William Chan, Jonathan Ho, and Mohammad Norouzi. Learning fast samplers for diffusion models by differentiating through sample quality. In *International Conference on Learning Representations*, 2021.

Zhisheng Xiao, Karsten Kreis, and Arash Vahdat. Tackling the generative learning trilemma with denoising diffusion gans. *arXiv preprint arXiv:2112.07804*, 2021.

Fisher Yu, Ari Seff, Yinda Zhang, Shuran Song, Thomas Funkhouser, and Jianxiong Xiao. Lsun: Construction of a large-scale image dataset using deep learning with humans in the loop. *arXiv preprint arXiv:1506.03365*, 2015.

Shengjia Zhao, Hongyu Ren, Arianna Yuan, Jiaming Song, Noah Goodman, and Stefano Ermon. Bias and generalization in deep generative models: An empirical study. *Advances in Neural Information Processing Systems*, 31, 2018.

Huangjie Zheng, Pengcheng He, Weizhu Chen, and Mingyuan Zhou. Truncated diffusion probabilistic models. *arXiv preprint arXiv:2202.09671*, 2022.

Linqi Zhou, Yilun Du, and Jiajun Wu. 3d shape generation and completion through point-voxel diffusion. In *Proceedings of the IEEE/CVF International Conference on Computer Vision*, pp. 5826–5835, 2021.

A Appendix

A.1 ELBO Proof

Prove

$$\log p(\mathbf{x}^0) \geq -(L_{\text{VAE}} + L_{\text{DDPM}}) \quad (13)$$

in Equation 7 in the main text.

Proof. Through variational inference, we have

$$\log p(\mathbf{x}^0) = \log \int p(\mathbf{x}^{0:T'}, \mathbf{z}) d\mathbf{x}^{1:T'} d\mathbf{z} \quad (14)$$

$$= \log \int q(\mathbf{x}^{1:T'}, \mathbf{z} | \mathbf{x}^0) \frac{p(\mathbf{x}^{0:T'}, \mathbf{z})}{q(\mathbf{x}^{1:T'}, \mathbf{z} | \mathbf{x}^0)} d\mathbf{x}^{1:T'} d\mathbf{z} \quad (15)$$

$$\geq \int q(\mathbf{x}^{1:T'}, \mathbf{z} | \mathbf{x}^0) \log \frac{p(\mathbf{x}^{0:T'}, \mathbf{z})}{q(\mathbf{x}^{1:T'}, \mathbf{z} | \mathbf{x}^0)} d\mathbf{x}^{1:T'} d\mathbf{z} \quad (16)$$

$$= \mathbb{E}_{q(\mathbf{x}^{1:T'}, \mathbf{z} | \mathbf{x}^0)} \log \frac{p(\mathbf{x}^{0:T'}, \mathbf{z})}{q(\mathbf{x}^{1:T'}, \mathbf{z} | \mathbf{x}^0)}. \quad (17)$$

This is because \log is a concave function and

$$\int q(\mathbf{x}^{1:T'}, \mathbf{z} | \mathbf{x}^0) d\mathbf{x}^{1:T'} d\mathbf{z} = 1. \quad (18)$$

We plug in the definition that

$$p(\mathbf{x}^{0:T'}, \mathbf{z}) = p(\mathbf{z}) p_\phi(\mathbf{x}^{T'} | \mathbf{z}) p_\theta(\mathbf{x}^{0:(T'-1)} | \mathbf{x}^{T'}), \quad (19)$$

$$q(\mathbf{x}^{1:T'}, \mathbf{z} | \mathbf{x}^0) = q(\mathbf{x}^{1:T'} | \mathbf{x}^0) q_\psi(\mathbf{z} | \mathbf{x}^0) \quad (20)$$

and obtain

$$\log p(\mathbf{x}^0) \geq \mathbb{E}_{q(\mathbf{x}^{1:T'}, \mathbf{z} | \mathbf{x}^0)} \log \frac{p(\mathbf{z}) p_\phi(\mathbf{x}^{T'} | \mathbf{z}) p_\theta(\mathbf{x}^{0:(T'-1)} | \mathbf{x}^{T'})}{q(\mathbf{x}^{1:T'} | \mathbf{x}^0) q_\psi(\mathbf{z} | \mathbf{x}^0)} \quad (21)$$

$$= \mathbb{E}_{q(\mathbf{x}^{1:T'}, \mathbf{z} | \mathbf{x}^0)} \left[\log \frac{p(\mathbf{z})}{q_\psi(\mathbf{z} | \mathbf{x}^0)} + \log \frac{p_\phi(\mathbf{x}^{T'} | \mathbf{z}) p_\theta(\mathbf{x}^{0:(T'-1)} | \mathbf{x}^{T'})}{q(\mathbf{x}^{1:T'} | \mathbf{x}^0)} \right]. \quad (22)$$

We set the loss function as

$$L = -\mathbb{E}_{q(\mathbf{x}^{1:T'}, \mathbf{z}|\mathbf{x}^0)} \left[\log \frac{p(\mathbf{z})}{q_\psi(\mathbf{z}|\mathbf{x}^0)} + \log \frac{p_\phi(\mathbf{x}^{T'}|\mathbf{z})p_\theta(\mathbf{x}^{0:(T'-1)}|\mathbf{x}^{T'})}{q(\mathbf{x}^{1:T'}|\mathbf{x}^0)} \right]. \quad (23)$$

The first term is:

$$L_1 = -\mathbb{E}_{q(\mathbf{x}^{1:T'}, \mathbf{z}|\mathbf{x}^0)} \log \frac{p(\mathbf{z})}{q_\psi(\mathbf{z}|\mathbf{x}^0)} \quad (24)$$

$$= \mathbb{E}_{q(\mathbf{x}^{1:T'}, \mathbf{z}|\mathbf{x}^0)} \log \frac{q_\psi(\mathbf{z}|\mathbf{x}^0)}{p(\mathbf{z})} \quad (25)$$

$$= \mathbb{E}_{q(\mathbf{x}^{1:T'}|\mathbf{x}^0)q_\psi(\mathbf{z}|\mathbf{x}^0)} \log \frac{q_\psi(\mathbf{z}|\mathbf{x}^0)}{p(\mathbf{z})} \quad (26)$$

$$= D_{\text{KL}}(q_\psi(\mathbf{z}|\mathbf{x}^0)||p(\mathbf{z})). \quad (27)$$

The second term is:

$$L_2 = -\mathbb{E}_{q(\mathbf{x}^{1:T'}, \mathbf{z}|\mathbf{x}^0)} \log \frac{p_\phi(\mathbf{x}^{T'}|\mathbf{z})p_\theta(\mathbf{x}^{0:(T'-1)}|\mathbf{x}^{T'})}{q(\mathbf{x}^{1:T'}|\mathbf{x}^0)} \quad (28)$$

$$= \mathbb{E}_{q(\mathbf{x}^{1:T'}, \mathbf{z}|\mathbf{x}^0)} \log \frac{q(\mathbf{x}^{1:T'}|\mathbf{x}^0)}{p_\phi(\mathbf{x}^{T'}|\mathbf{z})p_\theta(\mathbf{x}^{0:(T'-1)}|\mathbf{x}^{T'})} \quad (29)$$

$$= \mathbb{E}_{q(\mathbf{x}^{1:T'}, \mathbf{z}|\mathbf{x}^0)} \left[\log \frac{\prod_{t=1}^{T'} q(\mathbf{x}^t|\mathbf{x}^{t-1})}{\prod_{t=1}^{T'} p_\theta(\mathbf{x}^{t-1}|\mathbf{x}^t)} - \log p_\phi(\mathbf{x}^{T'}|\mathbf{z}) \right] \quad (30)$$

$$= \mathbb{E}_{q(\mathbf{x}^{1:T'}, \mathbf{z}|\mathbf{x}^0)} \left[\sum_{t=1}^{T'} \log \frac{q(\mathbf{x}^t|\mathbf{x}^{t-1})}{p_\theta(\mathbf{x}^{t-1}|\mathbf{x}^t)} - \log p_\phi(\mathbf{x}^{T'}|\mathbf{z}) \right] \quad (31)$$

$$= \mathbb{E}_{q(\mathbf{x}^{1:T'}, \mathbf{z}|\mathbf{x}^0)} \left[\sum_{t=2}^{T'} \log \frac{q(\mathbf{x}^t|\mathbf{x}^{t-1})}{p_\theta(\mathbf{x}^{t-1}|\mathbf{x}^t)} + \log \frac{q(\mathbf{x}^1|\mathbf{x}^0)}{p_\theta(\mathbf{x}^0|\mathbf{x}^1)} - \log p_\phi(\mathbf{x}^{T'}|\mathbf{z}) \right] \quad (32)$$

$$= \mathbb{E}_{q(\mathbf{x}^{1:T'}, \mathbf{z}|\mathbf{x}^0)} \left[\sum_{t=2}^{T'} \log \left(\frac{q(\mathbf{x}^{t-1}|\mathbf{x}^t, \mathbf{x}^0)}{p_\theta(\mathbf{x}^{t-1}|\mathbf{x}^t)} \frac{q(\mathbf{x}^t|\mathbf{x}^0)}{q(\mathbf{x}^{t-1}|\mathbf{x}^0)} \right) + \log \frac{q(\mathbf{x}^1|\mathbf{x}^0)}{p_\theta(\mathbf{x}^0|\mathbf{x}^1)} - \log p_\phi(\mathbf{x}^{T'}|\mathbf{z}) \right] \quad (33)$$

$$= \mathbb{E}_{q(\mathbf{x}^{1:T'}, \mathbf{z}|\mathbf{x}^0)} \left[\sum_{t=2}^{T'} \log \frac{q(\mathbf{x}^{t-1}|\mathbf{x}^t, \mathbf{x}^0)}{p_\theta(\mathbf{x}^{t-1}|\mathbf{x}^t)} + \sum_{t=2}^{T'} \log \frac{q(\mathbf{x}^t|\mathbf{x}^0)}{q(\mathbf{x}^{t-1}|\mathbf{x}^0)} + \log \frac{q(\mathbf{x}^1|\mathbf{x}^0)}{p_\theta(\mathbf{x}^0|\mathbf{x}^1)} - \log p_\phi(\mathbf{x}^{T'}|\mathbf{z}) \right] \quad (34)$$

$$= \mathbb{E}_{q(\mathbf{x}^{1:T'}, \mathbf{z}|\mathbf{x}^0)} \left[\sum_{t=2}^{T'} \log \frac{q(\mathbf{x}^{t-1}|\mathbf{x}^t, \mathbf{x}^0)}{p_\theta(\mathbf{x}^{t-1}|\mathbf{x}^t)} + \log \frac{q(\mathbf{x}^{T'}|\mathbf{x}^0)}{q(\mathbf{x}^1|\mathbf{x}^0)} + \log \frac{q(\mathbf{x}^1|\mathbf{x}^0)}{p_\theta(\mathbf{x}^0|\mathbf{x}^1)} - \log p_\phi(\mathbf{x}^{T'}|\mathbf{z}) \right] \quad (35)$$

$$= \mathbb{E}_{q(\mathbf{x}^{1:T'}, \mathbf{z}|\mathbf{x}^0)} \left[\sum_{t=2}^{T'} \log \frac{q(\mathbf{x}^{t-1}|\mathbf{x}^t, \mathbf{x}^0)}{p_\theta(\mathbf{x}^{t-1}|\mathbf{x}^t)} + \log q(\mathbf{x}^{T'}|\mathbf{x}^0) - \log p_\theta(\mathbf{x}^0|\mathbf{x}^1) - \log p_\phi(\mathbf{x}^{T'}|\mathbf{z}) \right] \quad (36)$$

$$= \mathbb{E}_{q(\mathbf{x}^{1:T'}, \mathbf{z}|\mathbf{x}^0)} \left[\log \frac{q(\mathbf{x}^t|\mathbf{x}^0)}{p_\phi(\mathbf{x}^{T'}|\mathbf{z})} + \sum_{t=2}^{T'} \log \frac{q(\mathbf{x}^{t-1}|\mathbf{x}^t, \mathbf{x}^0)}{p_\theta(\mathbf{x}^{t-1}|\mathbf{x}^t)} - \log p_\theta(\mathbf{x}^0|\mathbf{x}^1) \right] \quad (37)$$

$$= \mathbb{E}_{q(\mathbf{x}^{1:T'}, \mathbf{z}|\mathbf{x}^0)} \log \frac{q(\mathbf{x}^t|\mathbf{x}^0)}{p_\phi(\mathbf{x}^{T'}|\mathbf{z})} + L_{\text{DDPM}}, \quad (38)$$

where Line 33 is because

$$q(\mathbf{x}^t|\mathbf{x}^{t-1})q(\mathbf{x}^{t-1}|\mathbf{x}^0) = q(\mathbf{x}^{t-1}, \mathbf{x}^t|\mathbf{x}^0) = q(\mathbf{x}^{t-1}|\mathbf{x}^t, \mathbf{x}^0)q(\mathbf{x}^t|\mathbf{x}^0) \implies \quad (39)$$

$$q(\mathbf{x}^t|\mathbf{x}^{t-1}) = \frac{q(\mathbf{x}^{t-1}|\mathbf{x}^t, \mathbf{x}^0)q(\mathbf{x}^t|\mathbf{x}^0)}{q(\mathbf{x}^{t-1}|\mathbf{x}^0)}, \quad (40)$$

and

$$L_{\text{DDPM}} = \mathbb{E}_{q(\mathbf{x}^{1:T'}, \mathbf{z} | \mathbf{x}^0)} \left[\sum_{t=2}^{T'} \log \frac{q(\mathbf{x}^{t-1} | \mathbf{x}^t, \mathbf{x}^0)}{p_\theta(\mathbf{x}^{t-1} | \mathbf{x}^t)} - \log p_\theta(\mathbf{x}^0 | \mathbf{x}^1) \right] \quad (41)$$

$$= \sum_{t=2}^{T'} \mathbb{E}_{q(\mathbf{x}^{1:T'}, \mathbf{z} | \mathbf{x}^0)} \log \frac{q(\mathbf{x}^{t-1} | \mathbf{x}^t, \mathbf{x}^0)}{p_\theta(\mathbf{x}^{t-1} | \mathbf{x}^t)} - \mathbb{E}_{q(\mathbf{x}^{1:T'}, \mathbf{z} | \mathbf{x}^0)} \log p_\theta(\mathbf{x}^0 | \mathbf{x}^1) \quad (42)$$

$$= \sum_{t=2}^{T'} \mathbb{E}_{q(\mathbf{x}^t | \mathbf{x}^0) q(\mathbf{x}^{t-1} | \mathbf{x}^0, \mathbf{x}^t) q(\mathbf{x}^{1:T'} \setminus \{\mathbf{x}^{t-1}, \mathbf{x}^t\}, \mathbf{z} | \mathbf{x}^0, \mathbf{x}^{t-1}, \mathbf{x}^t)} \log \frac{q(\mathbf{x}^{t-1} | \mathbf{x}^t, \mathbf{x}^0)}{p_\theta(\mathbf{x}^{t-1} | \mathbf{x}^t)} \quad (43)$$

$$- \mathbb{E}_{q(\mathbf{x}^{2:T'}, \mathbf{z} | \mathbf{x}^0, \mathbf{x}^1) q(\mathbf{x}^1 | \mathbf{x}^0)} \log p_\theta(\mathbf{x}^0 | \mathbf{x}^1) \quad (44)$$

$$= \sum_{t=2}^{T'} \mathbb{E}_{q(\mathbf{x}^t | \mathbf{x}^0)} D_{\text{KL}}(q(\mathbf{x}^{t-1} | \mathbf{x}^t, \mathbf{x}^0) || p_\theta(\mathbf{x}^{t-1} | \mathbf{x}^t)) - \mathbb{E}_{q(\mathbf{x}^1 | \mathbf{x}^0)} \log p_\theta(\mathbf{x}^0 | \mathbf{x}^1). \quad (45)$$

The first term in L_2 is

$$\mathbb{E}_{q(\mathbf{x}^{1:T'}, \mathbf{z} | \mathbf{x}^0)} \log \frac{q(\mathbf{x}^{T'} | \mathbf{x}^0)}{p_\phi(\mathbf{x}^{T'} | \mathbf{z})} = \mathbb{E}_{q(\mathbf{x}^{1:(T'-1)}, \mathbf{z} | \mathbf{x}^0, \mathbf{x}^{T'}) q(\mathbf{x}^{T'} | \mathbf{x}^0)} \log \frac{q(\mathbf{x}^{T'} | \mathbf{x}^0)}{p_\phi(\mathbf{x}^{T'} | \mathbf{z})} \quad (46)$$

$$= \mathbb{E}_{q(\mathbf{x}^{1:(T'-1)}, \mathbf{z} | \mathbf{x}^0, \mathbf{x}^{T'})} D_{\text{KL}}(q(\mathbf{x}^{T'} | \mathbf{x}^0) || p_\phi(\mathbf{x}^{T'} | \mathbf{z})) \quad (47)$$

$$= \mathbb{E}_{q(\mathbf{x}^{1:(T'-1)} | \mathbf{x}^0, \mathbf{x}^{T'}, \mathbf{z}) q(\mathbf{z} | \mathbf{x}^0, \mathbf{x}^{T'})} D_{\text{KL}}(q(\mathbf{x}^{T'} | \mathbf{x}^0) || p_\phi(\mathbf{x}^{T'} | \mathbf{z})) \quad (48)$$

$$= \mathbb{E}_{q_\psi(\mathbf{z} | \mathbf{x}^0)} D_{\text{KL}}(q(\mathbf{x}^{T'} | \mathbf{x}^0) || p_\phi(\mathbf{x}^{T'} | \mathbf{z})). \quad (49)$$

Now the total loss is

$$L = L_1 + L_2 \quad (50)$$

$$= D_{\text{KL}}(q_\psi(\mathbf{z} | \mathbf{x}^0) || p(\mathbf{z})) + \mathbb{E}_{q_\psi(\mathbf{z} | \mathbf{x}^0)} D_{\text{KL}}(q(\mathbf{x}^{T'} | \mathbf{x}^0) || p_\phi(\mathbf{x}^{T'} | \mathbf{z})) + L_{\text{DDPM}} \quad (51)$$

$$= L_{\text{VAE}} + L_{\text{DDPM}}, \quad (52)$$

where L_{VAE} is defined as

$$L_{\text{VAE}} = D_{\text{KL}}(q_\psi(\mathbf{z} | \mathbf{x}^0) || p(\mathbf{z})) + \mathbb{E}_{q_\psi(\mathbf{z} | \mathbf{x}^0)} D_{\text{KL}}(q(\mathbf{x}^{T'} | \mathbf{x}^0) || p_\phi(\mathbf{x}^{T'} | \mathbf{z})). \quad (53)$$

We have finished the proof that

$$\log p(\mathbf{x}^0) \geq -L = -(L_{\text{VAE}} + L_{\text{DDPM}}). \quad (54)$$

□

A.2 Conditional Generation

In the case of conditional generation, we use \mathbf{c} to denote the condition. It contains some information about the clean image \mathbf{x}^0 . For example, \mathbf{c} could be the class of \mathbf{x}^0 , a low resolution image of \mathbf{x}^0 , or a grayscale image of \mathbf{x}^0 .

We adapt the encoding process in Equation 3 to

$$q(\mathbf{x}^{1:T'}, \mathbf{z} | \mathbf{x}^0, \mathbf{c}) = q(\mathbf{x}^{1:T'} | \mathbf{x}^0, \mathbf{c}) q_\psi(\mathbf{z} | \mathbf{x}^{1:T'}, \mathbf{x}^0, \mathbf{c}) = q(\mathbf{x}^{1:T'} | \mathbf{x}^0) q_\psi(\mathbf{z} | \mathbf{c}), \quad (55)$$

where $q_\psi(\mathbf{z} | \mathbf{c})$ is the encoder. We set it to be a Gaussian distribution whose mean and standard deviation are parameterized by a neural network. $q(\mathbf{x}^{1:T'} | \mathbf{x}^0)$ is the same as Equation 4. We then adapt the sampling process in Equation 5 to

$$p(\mathbf{x}^{0:T'}, \mathbf{z} | \mathbf{c}) = p(\mathbf{z}) p_\phi(\mathbf{x}^{T'} | \mathbf{z}, \mathbf{c}) p_\theta(\mathbf{x}^{0:(T'-1)} | \mathbf{x}^{T'}, \mathbf{c}), \quad (56)$$

where $p(\mathbf{z})$ is assumed to follow standard Gaussian distribution, $p_\phi(\mathbf{x}^{T'}|\mathbf{z}, \mathbf{c})$ is the decoder parameterized by a neural network, and $p_\theta(\mathbf{x}^{0:(T'-1)}|\mathbf{x}^{T'}, \mathbf{c})$ is the reverse process of the partial diffusion process in Equation 4. It is defined as

$$p_\theta(\mathbf{x}^{0:(T'-1)}|\mathbf{x}^{T'}, \mathbf{c}) = \prod_{t=1}^{T'} p_\theta(\mathbf{x}^{t-1}|\mathbf{x}^t, \mathbf{c}), \text{ where } p_\theta(\mathbf{x}^{t-1}|\mathbf{x}^t, \mathbf{c}) = \mathcal{N}(\mathbf{x}^{t-1}; \boldsymbol{\mu}_\theta(\mathbf{x}^t, \mathbf{c}, t), \sigma_t^2 \mathbf{I}). \quad (57)$$

Through variational inference, we can prove that

$$\log p(\mathbf{x}^0|\mathbf{c}) \geq -(L_{\text{VAE}} + L_{\text{DDPM}}), \quad (58)$$

$$\text{where } L_{\text{VAE}} = D_{\text{KL}}(q_\psi(\mathbf{z}|\mathbf{c})||p(\mathbf{z})) + \mathbb{E}_{q_\psi(\mathbf{z}|\mathbf{x}^0)} D_{\text{KL}}(q(\mathbf{x}^{T'}|\mathbf{x}^0)||p_\phi(\mathbf{x}^{T'}|\mathbf{z}, \mathbf{c})), \quad (59)$$

$$L_{\text{DDPM}} = \sum_{t=2}^{T'} \mathbb{E}_{q(\mathbf{x}^t|\mathbf{x}^0)} D_{\text{KL}}(q(\mathbf{x}^{t-1}|\mathbf{x}^t, \mathbf{x}^0)||p_\theta(\mathbf{x}^{t-1}|\mathbf{x}^t, \mathbf{c})) - \mathbb{E}_{q(\mathbf{x}^1|\mathbf{x}^0)} \log p_\theta(\mathbf{x}^0|\mathbf{x}^1, \mathbf{c}). \quad (60)$$

The proof is the same as Section A.1. Now we have two loss terms, L_{DDPM} and L_{VAE} . This means that we can train a conditional DDPM and a VAE-like model separately, and then combine them together to obtain a conditional generative model. First, The loss term L_{DDPM} is the same of a normal conditional DDPM, except that we do not need to train the full chain range from 1 to T . Instead, we only need to train the first several steps range from 1 to T' .

Next, we will show that the loss term L_{VAE} amounts to train a VAE-like conditional generative model. Similarly to Equation 11, we can set $p_\phi(\mathbf{x}^{T'}|\mathbf{z}, \mathbf{c})$ to

$$p_\phi(\mathbf{x}^{T'}|\mathbf{z}, \mathbf{c}) \sim N(\mathbf{x}^{T'}; \sqrt{\bar{\alpha}_t} \mathbf{f}_\phi(\mathbf{z}, \mathbf{c}), (1 - \bar{\alpha}_t) \mathbf{I}). \quad (61)$$

Then

$$D_{\text{KL}}(q(\mathbf{x}^{T'}|\mathbf{x}^0)||p_\phi(\mathbf{x}^{T'}|\mathbf{z}, \mathbf{c})) = C_1 \|\mathbf{x}^0 - \mathbf{f}_\phi(\mathbf{z}, \mathbf{c})\|^2 + C_2, \quad (62)$$

where C_1, C_2 are some scalar constants. Now the second term in L_{VAE} means that the decoder $\mathbf{f}_\phi(\mathbf{z}, \mathbf{c})$ need to reconstruct the original image \mathbf{x}^0 , based on the latent code \mathbf{z} sampled from the encoder $q_\psi(\mathbf{z}|\mathbf{c})$ and the condition \mathbf{c} . Therefore, L_{VAE} can be optimized by following a similar procedure to train a VAE on clean images \mathbf{x}^0 , except that we need to change the input of the encoder q_ψ from \mathbf{x}^0 to \mathbf{c} , and allow the decoder \mathbf{f}_ϕ to utilize the condition \mathbf{c} when reconstructing the original image \mathbf{x}^0 .

Sampling Procedure. After training the conditional DDPM and the VAE-like model separately, we can combine them to form a conditional generative model. We can use the following equation to generate samples given condition \mathbf{c} :

$$p(\mathbf{x}^{0:T'}, \mathbf{z}|\mathbf{c}) = q_\psi(\mathbf{z}|\mathbf{c}) p_\phi(\mathbf{x}^{T'}|\mathbf{z}, \mathbf{c}) p_\theta(\mathbf{x}^{0:(T'-1)}|\mathbf{x}^{T'}, \mathbf{c}). \quad (63)$$

First sample the latent code \mathbf{z} from $q_\psi(\mathbf{z}|\mathbf{c})$, then use the decoder of the VAE to generate an image $\mathbf{f}_\phi(\mathbf{z}, \mathbf{c})$. Next, sample $\mathbf{x}^{T'}$ from the distribution described in Equation 61. Finally, use the DDPM to sample \mathbf{x}^{t-1} from $p_\theta(\mathbf{x}^{t-1}|\mathbf{x}^t, \mathbf{c})$ for $t = T', T' - 1, \dots, 1$, and output the generated image \mathbf{x}^0 .

During sampling, we do not need to restrict how $\mathbf{f}_\phi(\mathbf{z}, \mathbf{c})$ is trained, or what kind of model it is. It could be a conditional GAN or any other conditional generation model.

A.3 Computational Cost

On the CelebA dataset, we train the StyleGAN2, the ES-DDPM and the full-length DDPM on 8 NVIDIA RTX 2080Ti GPUs. For CelebA-64, the StyleGAN2 and the full-length DDPM are trained for 10^5 (around 25 hours) iterations and 9×10^5 (around 80 hours) respectively. For CelebA-128, the StyleGAN2 and the full-length DDPM are trained for 2.4×10^5 (around 183 hours) iterations and 4×10^6 (around 448 hours) respectively. As for ES-DDPMs, their training time of each iteration is the same as full-length DDPMs and can be inferred from Figure 2. For image generation experiments,

it takes around one day for the 1000-step DDPM to generate 50000 random Celeba-128 images on 8 NVIDIA RTX 2080Ti GPUs. Other image generation experiment on CelebA takes less time.

For the ImageNet-64 dataset, we use pre-trained DDPM models and pre-generated BigGAN-deep images from the work (Dhariwal & Nichol, 2021). It takes about 8 hours for the 250-step DDPM to generate 50000 random images on 4 NVIDIA A100 GPUs. Generation time of different length ES-DDPMs can be inferred accordingly.

For LSUN-Bedroom and LSUN-Cat datasets, we use pre-trained DDPM models and pre-generated StyleGAN images from the work (Dhariwal & Nichol, 2021). It takes about one day for the 1000-step DDPM to generate 50000 random LSUN-Bedroom or LSUN-Cat images on 24 NVIDIA A100 GPUs. Generation time of different length ES-DDPMs can be inferred accordingly.

A.4 DDPM Acceleration Experiment Results on LSUN Datasets

Table 8: FID comparison of different DDPM acceleration methods on the LSUN-Bedroom dataset.

Denosing Steps	500	100	50	20	10	5
ES-DDPM($T' = 100$)+StyleGAN+TR(Ours)		1.85	1.83	2.03	2.67	3.84
DDIM (Song et al., 2020)		6.62	6.75	8.89	16.95	
PNDM (Liu et al., 2022)		6.91	6.44	5.68	6.99	12.6
FastDPM (Kong & Ping, 2021)		7.98	8.37	9.86	19.07	
TDPM-GAN (Zheng et al., 2022)	3.95		4.10			
TDPM-CT (Zheng et al., 2022)	4.01		4.95			

Table 9: FID comparison of different DDPM acceleration methods on the LSUN-Cat dataset. “*” means the images for evaluation are generated by ourselves for this method.

Denosing Steps	100	50	20	10	5
ES-DDPM($T' = 100$)+StyleGAN2+TR(Ours)	5.47	5.88	7.27	9.72	13.48
DDIM* (Song et al., 2020)	7.43	8.80	12.40	20.11	48.39
TR* (Nichol & Dhariwal, 2021)	9.88	14.60	28.86	56.62	114.00

A.5 Additional Controllable Generation Experiments



Figure 4: On CelebA-128, ES-DDPM can preserve high-level semantics in the images generated by StyleGAN2 for not too large T' 's. Hence our combined model can control high-level semantics such as gender and age in generated images.

Figure 4 shows that we can use StyleGAN2 to control the age and the gender of the generated face, and the ES-DDPM can preserve these high-level semantic information. In this way, we can control high-level semantics for our combined model. Other works (Preechakul et al., 2021; Pandey et al., 2022) have also shown that it is possible to combine DDPMs and VAEs to control high-level semantics of the generated images. Compared with them, our method can achieve better sample quality using the same number of denoising steps as shown in Table 2 and Table 6. In addition, these methods need to alter the training process of the DDPM and train a DDPM that is specific to the other



Figure 5: On LSUN-Cat-256, we perform stroke-based local editing on StyleGAN2 generated cats. ES-DDPM($T' = 300$) can refine the editing we made and remove artifacts.

model they want to combine DDPM with. On the contrary, our method can combine a pre-trained DDPM with any other generative model that has the ability to control high-level semantics to achieve high-level controllable generation for the DDPM.

Figure 5 shows that we can perform stroke-based local editing on the cat images generated by StyleGAN2, and then use the ES-DDPM to refine it, mitigate artifacts and make the images photo-realistic. This local editing technique is the same as the one proposed in the work (Meng et al., 2021).